Disordered Assembly of MFI Zeolite Nanosheets with a Large Volume of Intersheet Mesopores

ARTICLE *in* CHEMISTRY OF MATERIALS · JANUARY 2011

Impact Factor: 8.35 · DOI: 10.1021/cm103245m

4 AUTHORS, INCLUDING:

Kyungsu Na
Korea Advanced Institute of Science and Tec…
16 PUBLICATIONS **1,320** CITATIONS
SEE PROFILE

Woojin Park
Korea Advanced Institute of Science and Tec…
5 PUBLICATIONS **318** CITATIONS
SEE PROFILE

Yongbeom Seo
Institute for Basic Science
20 PUBLICATIONS **552** CITATIONS
SEE PROFILE

CHEMISTRY OF MATERIALS

ARTICLE

pubs.acs.org/cm

Disordered Assembly of MFI Zeolite Nanosheets with a Large Volume of Intersheet Mesopores

Kyungsu Na,[†] Woojin Park,[†,‡] Yongbeom Seo,[†,‡] and Ryong Ryoo*[,†,‡]

[†]Center for Functional Nanomaterials, Department of Chemistry, KAIST, Daejeon 305-701, Korea

[‡]Graduate School of Nanoscience and Technology (WCU), KAIST, Daejeon 305-701, Korea

ABSTRACT: MFI zeolite nanosheets with a single-unit-cell crystal thickness were synthesized under hydrothermal synthesis conditions using diquaternary ammonium surfactants as the zeolite structure-generating agent. The zeolite structure generation process was analyzed from X-ray powder diffraction, N_2 adsorption isotherms, scanning electron micrographs, and transmission electron micrographs of the porous materials generated at various reaction times. This analysis indicated that the nanosheets were initially generated as a disordered assembly that transformed into an ordered multilamellar mesostructure through a dissolution−recrystallization process upon prolonged hydrothermal aging. Synthesis factors affecting the rates of the initial generation of the nanosheets and their restructuring process were investigated while varying the temperature, structure of the surfactant tail, synthesis compositions, and basicity. On the basis of the result, it was possible to synthesize MFI zeolite nanosheets as a fully disordered assembly possessing a large mesopore volume even under synthesis conditions using the bromide form of the surfactant and a sodium-containing silica source such as water glass.

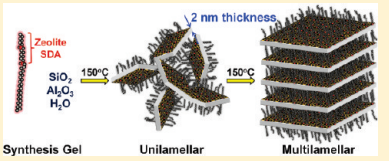

KEYWORDS: single unit cell thickness, MFI zeolite nanosheet, unilamellar, multilamellar, mesoporous zeolite, hierarchical zeolite, zeolite MFI, organic surfactant, mesoporous silica

INTRODUCTION

Zeolite is a family of crystalline microporous aluminosilicate minerals of various structure types with distinct pore dimensions, pore connectivity, and framework compositions.[1−4] Zeolite is widely used as a molecular shape-selective adsorbent and catalyst.[3,4] Specific structure types of zeolite with suitable pore mouths can be selected for given adsorbates. Some types of zeolite are naturally found as minerals, but for catalytic applications, most are synthesized in polycrystalline powder forms with a crystal thickness of about several micrometers or less. Micropore mouths in zeolite (<1 nm in diameter) are normally much smaller than the crystallite thickness. Because of the long diffusion pathways through crystalline domains, zeolite is commonly associated with diffusion limitations for catalytic applications and adsorption.[3−5]

A strategy to overcome the diffusion limitations in zeolite is to decrease the crystal size to the nanoparticle range, e.g., less than 50 nm.[6] Zeolite samples composed of such nanoparticles have intercrystalline mesopores that serve as a highway for the facile diffusion of adsorbates into micropores. An alternative approach is to generate intracrystalline mesopores (2−50 nm) in micrometer-size zeolite particles so that diffusion into micropores can rapidly occur through mesopores. Intracrystalline mesopores can be generated in a zeolite particle via postsynthesis dealumination or a desilication process.[7−10] The addition of mesopore-generating agents such as carbon nanoparticles,[11−14] polymer beads,[15,16] and organosilane surfactants[17] into a zeolite synthesis composition is also effective for the synthesis of zeolite with intracrystalline mesopores. Microporous zeolites with mesopores generated in this manner are often referred to as "hierarchically microporous-mesoporous" or "hierarchical" zeolites. Hierarchically porous zeolites have the advantage of facile diffusion into (and also out of) catalytic active sites to permit reactions to take place inside micropores.[18−20] The mesopore walls also provide sufficient catalytic active sites for the conversion of bulky molecules.[21]

Recently, a synthesis strategy for MFI zeolite nanosheets with a single-unit-cell crystal thickness was developed in the laboratory of the present authors using a diquaternary ammonium-type surfactant with the formula of $C_{22}H_{45}-N^+(CH_3)_2-C_6H_{12}-N^+(CH_3)_2-C_6H_{13}$ (designated by C_{22-6-6}).[22] The MFI nanosheets synthesized in this manner were wide in the $a-c$ plane and 2 nm thick along the b axis. When zeolite synthesis was performed with $C_{22-6-6}Br_2$ under a Na^+-rich condition, the nanosheets were regularly stacked with equal spacings corresponding to the surfactant tail.[22,23] The zeolite assembly was referred to as *multilamellar* MFI nanosheets. The nanosheets in this mesostructure coalesced to each other when the surfactant was removed by calcination, leading to a significant loss of intersheet mesoporosity. On the other hand, when zeolite synthesis was performed with $C_{22-6-6}(OH)_2$ under a Na^+-free condition, the nanosheets were obtained in the form of a highly disordered assembly. This assembly was referred to as *unilamellar* MFI nanosheets because of its individually separated lamellar

Received: November 11, 2010
Revised: January 10, 2011
Published: January 31, 2011

structure. The unilamellar zeolite retained a large volume of intersheet mesopores after the surfactant was removed through high-temperature calcination in air. The unilamellar zeolite exhibited a remarkably enhanced lifetime as a catalyst for methanol-to-hydrocarbon conversion as compared with the bulk zeolite; this was attributed to facile diffusion in the hierarchically porous structure.[22] However, a unilamellar MFI zeolite was obtained in a limited synthesis condition requiring a long reaction time, $C_{22-6-6}(OH)_2$, and a Na^+-free silica source.

This study was undertaken to find a generalized synthesis condition for unilamellar MFI nanosheets using $C_{22-6-6}Br_2$ instead of $C_{22-6-6}(OH)_2$ and a low-cost silica source permitting a high concentration of Na^+. To do this, the zeolite intersheet structural correlation was investigated under various hydrothermal reaction times, temperatures, synthesis gel compositions, and surfactant tail lengths. From the result, we discovered that the nanosheets were assembled into a unilamellar mesostructure in the beginning of their formation, irrespective of the detailed synthesis conditions. The unilamellar assembly subsequently became a multilamellar assembly through a dissolution-recrystallization process. The lifetime of the unilamellar structure was very short or sufficiently long for product recovery before its transformation, depending on the differing synthesis conditions. We report the result because this information can lead to the synthesis of unilamellar MFI zeolite nanosheets possessing a large mesopore volume with a short reaction time, even under synthesis conditions using $C_{22-6-6}Br_2$ and a sodium silicate solution.

EXPERIMENTAL SECTION

Materials Synthesis. $C_{n-6-6}Br_2$ (n = 12, 16, or 22) surfactants were obtained following a synthesis procedure reported in the literature.[22,23] The compounds were identified by solution ^{1}H NMR. These compounds were used as synthesized or after they were converted to $C_{n-6-6}(OH)_2$ using anionic exchange resin. Fumed silica (Aerosil, Degussa) was purchased from Aldrich, tetraethylorthosilicate (TEOS, 95%) from Junsei, and water glass (29 wt % aqueous solution, Si/Na = 1.75) from Shinheung Silicate. $Al_2(SO_4)_3 \cdot 18\ H_2O$ (98%) was used as received from Aldrich. Sodium aluminate (43 wt % Na_2O, 53 wt % Al_2O_3, Na/Al = 1.06, Aldrich) was dissolved in doubly distilled water to prepare a 1.08×10^{-7} M solution, and the solution was quickly used for zeolite synthesis.

Zeolite synthesis using water glass as a silica source was tested at various gel compositions in the range of 100 SiO_2:5.0−15.0 $C_{n-6-6}Br_2$:(28.6 + 1.4 a) Na_2O:a Al_2O_3:18−27 H_2SO_4:4000 H_2O, where a = 0−1.7. Water glass containing 0.02 mol of SiO_2 was used in a typical synthesis batch. $C_{n-6-6}Br_2$ was dissolved in doubly distilled water to give a 3.05×10^{-7} M solution. The water glass solution was added to this surfactant solution at once under vigorous magnetic stirring at room temperature. A 1.08×10^{-7} M aqueous solution of sodium aluminate (for the desired Si/Al ratio) was then added dropwise under magnetic stirring. The resultant mixture remained homogeneous. The mixture was added at once with a 1.36×10^{-6} M sulfuric acid in a polypropylene bottle, for the given gel composition. The resultant mixture was immediately shaken by hand or with a mechanical stirrer very vigorously for 5 min to obtain as homogeneous a gel as possible. After further stirring for 6 h with a magnetic stirrer placed in an oven at 60 °C, the gel mixture was transferred to a Teflon-lined stainless steel autoclave. The autoclave was tumbled (60 rpm) in an oven maintained at 150 °C. Small amounts of sample were taken after temporarily cooling the autoclave. The samples were filtered and dried at 130 °C before analyses as *synthesized*. A small portion of each sample was calcined at 550 °C for 3 h under flowing air for analyses as *calcined*.

Synthesis experiments using fumed silica and TEOS were conducted on the basis of 0.02 mol of SiO_2, as in the case of water glass. Gel compositions were similar to the case of water glass, except that the Na concentration was extended to zero. The reactant mixing order proceeded in this case as follows. First, a 2.52×10^{-7} M aqueous solution of $C_{n-6-6}(OH)_2$ was prepared. Alternatively, $C_{n-6-6}Br_2$ and NaOH were dissolved in distilled water to obtain the same surfactant concentration ($\geq$2 NaOH/$C_{n-6-6}Br_2$). To the surfactant solution, $Al_2(SO_4)_3 \cdot 18\ H_2O$ was homogeneously dissolved. The silica source was then combined at once. The resultant mixture was immediately and vigorously shaken for 5 min. The remainder of the synthesis procedure was identical to that described above.

MCM-41[24] and bulk MFI zeolite[25] were synthesized in pure silica forms by following the procedure in the literature. TEOS was the silica source for both materials. Hexadecyltrimethylammonium bromide was used in the MCM-41 synthesis. Tetrapropylammonium hydroxide was used as the zeolite structure-directing agent for bulk MFI. The MCM-41 and MFI samples were calcined at 550 °C for 3 h under flowing air.

Characterization. Powder X-ray diffraction (XRD) patterns were recorded from a Rigaku Multiflex diffractometer equipped with a Cu Kα radiation (λ = 0.1541 nm) at 30 kV, 40 mA (1.2 kW). Scanning electron micrographs (SEM) were obtained with a FEI Nova 230 instrument operating at 2 kV in gentle-beam mode without a metal coating. Transmission electron micrographs (TEM) were taken with a Tecnai G2 F30 instrument with an accelerating voltage of 300 kV. N_2 adsorption−desorption isotherms were measured with a Micromeritics TriStar II volumetric adsorption analyzer at the liquid N_2 temperature (77 K). Prior to the adsorption measurements, all samples were degassed under a vacuum for 12 h at 573 K. The specific surface area was determined from the adsorption branch in the P/P_0 range between 0.05 and 0.20, using the Brunauer−Emmett−Teller (BET) equation. The pore size distributions were converted from the entire adsorption branch according to the Barrett−Joyner−Halenda (BJH) algorithm. The mechanical stability of samples was examined by following a procedure from the literature.[26] A calcined powder sample (50 mg) was compressed in a stainless steel die that was 10 mm in diameter. The mechanical stability was judged from the losses of the XRD intensity or the N_2 adsorption capacity that occurred due to compression.

RESULTS AND DISCUSSION

Generation of Unilamellar MFI under Na^+-Free Conditions. As the first basis for the synthesis of unilamellar MFI zeolite nanosheets, a hydrothermal reaction was performed with a gel composition of 100 SiO_2:15 $C_{22-6-6}(OH)_2$:1 Al_2O_3:3 H_2SO_4:6000 H_2O under a Na^+-free condition at 150 °C, as reported by Choi et al.[22] (see entry 1 in Table 1). Here, the zeolite structure-directing surfactant was $C_{22-6-6}(OH)_2$. Fumed silica was the silica source, and $Al_2(SO_4)_3 \cdot 18\ H_2O$ was used as an alumina precursor. Figure 1 displays the powder XRD patterns of the as-synthesized samples as a function of the reaction time over the period of 1−15 d. Sharp small-angle XRD peaks at 1 d show that the sample had an ordered hexagonal mesostructure that was similar to MCM-41 silica.[24,27] These peaks could be indexed to (10), (11), and (20) reflections, corresponding to the two-dimensional hexagonal structure. No atomic order was detected at this stage, as indicated by the absence of Bragg reflections in the wide-angle XRD. When the synthesis time was increased to 4 d, the (11) and (20) reflections in the small-angle region disappeared and the (10) peak was broadened. No Bragg reflections were noted at this stage in the wide-angle region. This result indicates that the initial MCM-41-like mesostructure transformed into a disordered mesostructure,

Table 1. Summary of Synthesis Conditions and Results

entry	SiO_2	H_2O	Na_2O	Al_2O_3	H_2SO_4	SDA type	SDA amount	reaction time (d)	mesostructure	S_{BET}[a] ($m^2\ g^{-1}$)	V_t[b] ($cm^3\ g^{-1}$)
1	100	6000	0	1	3	$C_{22-6-6}(OH)_2$	15	11	unilamellar	670	1.10
2	100	6000	0	1	3	$C_{16-6-6}(OH)_2$	15	12	unilamellar	650	0.90
3	100	4000	30	1	18	$C_{22-6-6}Br_2$	10	5	multilamellar	520	0.52
4	100	4000	30	1	24	$C_{22-6-6}Br_2$	7.5	3	unilamellar	660	1.00
5	100	4000	30	1	24	$C_{12-6-6}Br_2$	7.5	3	unilamellar	580	0.57
6	100	4000	30	1	24	$C_{16-6-6}Br_2$	7.5	3	unilamellar	610	0.71
7	100	4000	30	0	24	$C_{16-6-6}Br_2$	7.5	2	unilamellar	580	0.76
8	100	4000	30	1.7	18	$C_{16-6-6}Br_2$	7.5	10	unilamellar	578	0.50

[a] S_{BET} is the BET surface area ($m^2\ g^{-1}$) obtained from N_2 adsorption isotherm in the relative pressure range (P/P_0) of 0.05−0.20. [b] V_t is the total pore volume ($cm^3\ g^{-1}$) at relative pressure (P/P_0 = 0.97).

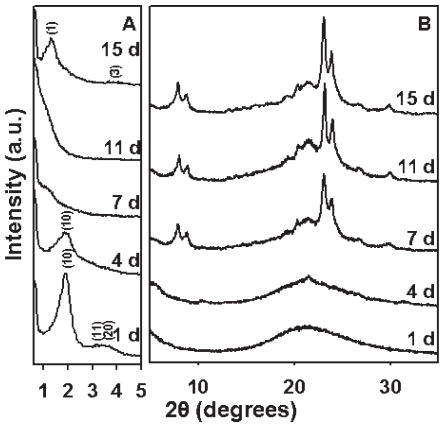

Figure 1. Small-angle (A) and wide-angle (B) powder XRD patterns of MFI zeolite nanosheets in the as-synthesized form periodically taken from the synthesis gel composition of 15 $C_{22-6-6}(OH)_2$:100 SiO_2:1 Al_2O_3:3 H_2SO_4:6000 H_2O after various hydrothermal reaction times.

similar to KIT-1 silica.[28] At 7 d, some Bragg reflections began to appear in the wide-angle XRD region. Most of the intense peaks could be indexed to the crystalline structure of MFI zeolite, but some peaks for MFI zeolites were missing. The small-angle peak disappeared almost completely. This indicated that we had unilamellar MFI nanosheets at this time. When the synthesis time was extended to 11 d, the XRD patterns were fully changed to those of the unilamellar MFI zeolite. The SEM and TEM images in Figure 2 are consistent with the XRD data discussed above. A hexagonal pore arrangement, as in MCM-41, was noted in TEM images of the sample collected at 1 d. The overall appearance of the 1 d sample indicated a sponge-like macroporous globular morphology. A fully crystalline structure with ultrathin nanosheet morphology was observed in the TEM images of the sample collected at 11 d. The individual MFI nanosheets were assembled irregularly, as reported by Choi et al.[22] Amorphous silica domains were not detected in the electron microscopic images.

Transformation of Unilamellar MFI into Multilamellar Assembly. As discussed above, high purity disordered unilamellar MFI zeolite was obtained after a reaction time of 11 d. When the product was aged for 15 d under the same synthesis condition at 150 °C, the wide-angle XRD pattern still indicated the formation of ultrathin MFI zeolite nanosheets. However, the small-angle XRD pattern changed to show two well-resolved Bragg reflections (Figure 1A), which were characteristic of an ordered multilamellar mesophase. The TEM image at 15 d in Figure 2 also shows regular stacking of nanosheets in the multilamellar MFI zeolite. In addition, the SEM image at 15 d showed morphologies with planar domains that were wider than those in the image at 11 d. The domain size of the individual nanosheets was somewhat narrow as compared with the multilamellar MFI zeolite obtained under the Na^+-rich condition.[22] Nevertheless, our result clarified that the ordered multilamellar MFI zeolite at 15 d was generated by the transformation from the disordered unilamellar MFI zeolite existing at 11 d.

The driving forces for the unilamellar−multilamellar reorganization process may be explained by the Ostwald ripening process taking place in the two-dimensional crystal domains due to the coupling with the hydrophobic interactions between surfactant tails. It is known that MFI zeolite crystals can grow through crystallization−dissolution processes reversibly under highly basic conditions, as in the present synthesis condition.[1,3] In our synthesis condition, however, crystal growth along the *b* axis would be forbidden because of the presence of bulk tails of the surfactant molecules covering the *a*−*c* planes. The crystal would thereby be confined to grow in the direction of the *a*−*c* plane. Moreover, this type of two-dimensional growth of the nanosheets would make the hydrophobic interaction of the surfactant tails between adjacent nanosheets progressively more favorable. The surface of the nanosheets should be densely covered by the long C_{22}-alkyl tails. This strongly hydrophobic surface may be stable if the surface area is extremely narrow or if the surface is well protected by another layer of free (not participating as SDA) surfactant molecules under the excessive presence of a surfactant. Accordingly, formation of the multilamellar mesophase would be a natural process that could lead to maximum interaction between hydrophobic tails. This is believed to cause the unilamellar−multilamellar reorganization process.

Effects of Surfactant Tail Length. The synthesis labeled as entry 2 in Table 1 was performed under the same condition used in entry 1, except for the substitution of $C_{22-6-6}(OH)_2$ with $C_{16-6-6}(OH)_2$. The XRD patterns of the product samples resulting from $C_{16-6-6}(OH)_2$ are displayed as a function of the reaction time in Figure 3. As this result shows, unilamellar nanosheets were obtained at 12 d by $C_{16-6-6}(OH)_2$. The zeolite generation at 12 d between $C_{22-6-6}(OH)_2$ and $C_{16-6-6}(OH)_2$ was nearly identical. However, the use of the two structure-directing agents resulted in a distinct difference at 15 d. In the case of $C_{22-6-6}(OH)_2$, the unilamellar MFI phase was mostly converted to the multilamellar phase, as mentioned above. In contrast, the $C_{16-6-6}(OH)_2$ result shows that the transformation did not occur during the same period. Small-angle reflections (Figure 3A) corresponding to multilamellar ordering did

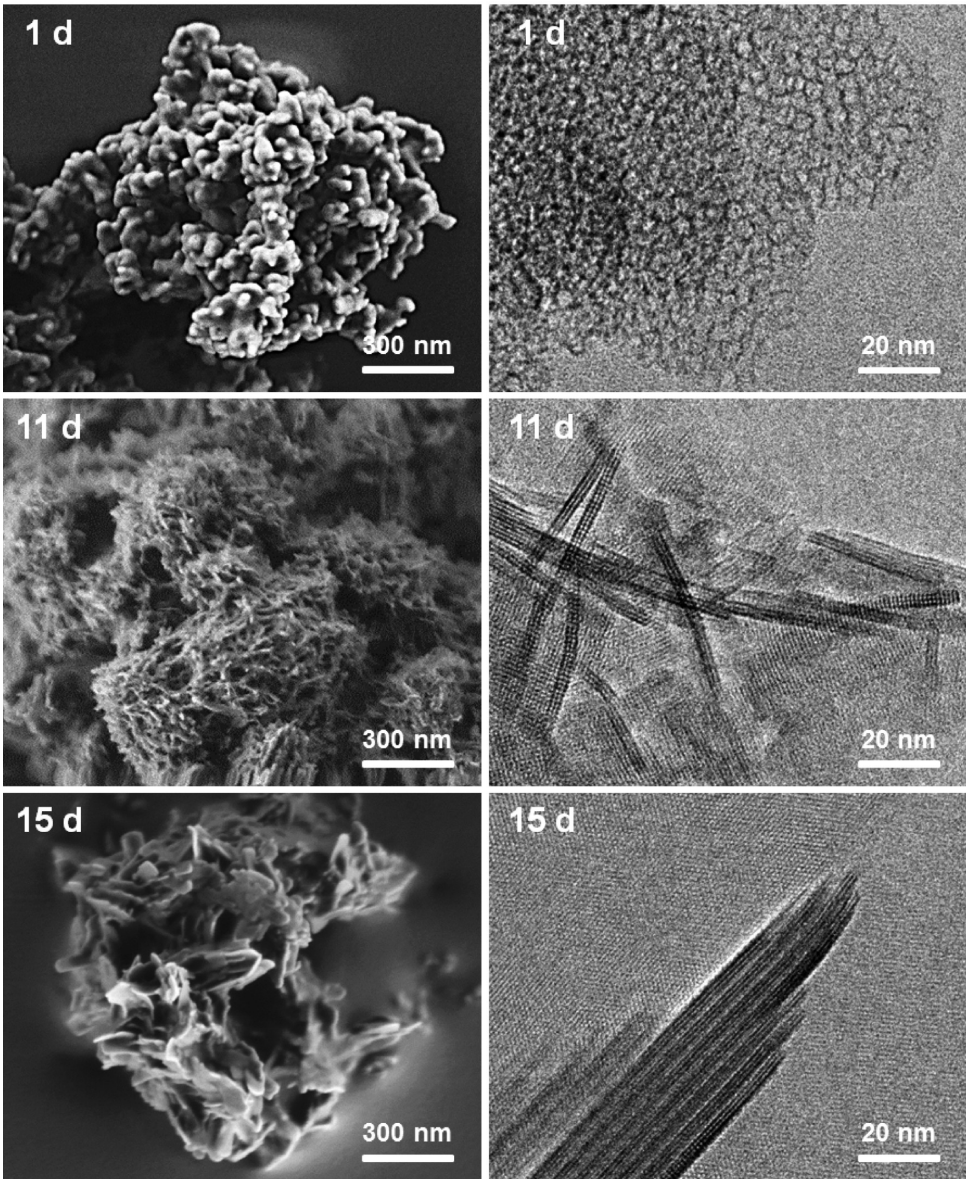

Figure 2. SEM (left column) and TEM (right column) images of MFI zeolite nanosheets in the as-synthesized form periodically taken from the synthesis gel composition of 15 $C_{22-6-6}(OH)_2$:100 SiO_2:1 Al_2O_3:3 H_2SO_4:6000 H_2O after various hydrothermal reaction times.

not reappear in the case of $C_{16-6-6}(OH)_2$. This indicates that the disordered unilamellar MFI zeolite product initially obtained at 12 d remained at 15 d. Thus, the transformation from a unilamellar to a multilamellar mesostructure could be suppressed when $C_{16-6-6}(OH)_2$ was used as the zeolite structure-directing agent in place of $C_{22-6-6}(OH)_2$. The suppression of the unilamellar-multilamellar transformation can be attributed to the relatively less hydrophobic character of the C_{16} alkyl tails as compared to the C_{22} alkyl tails. Because the narrow MFI nanosheets covered with C_{16} alkyl tails are less hydrophobic than those covered with C_{22} alkyl tails, transformation to the multilamellar mesophase was less favorable. The MFI nanosheets generated by $C_{16-6-6}(OH)_2$ at 12 d possessed a high BET surface area (650 $m^2 g^{-1}$), which was comparable to that (670 $m^2 g^{-1}$) of the MFI nanosheets collected at 11 d with $C_{22-6-6}(OH)_2$. The total pore volume was also very high (0.90 $cm^3 g^{-1}$) as compared to the multilamellar MFI samples with a lower volume of around 0.50 $cm^3 g^{-1}$.[22]

Despite the successful synthesis, the present synthesis was nevertheless performed under a Na^+-free condition using a hydroxide form of surfactant. In addition, the synthesis required a long crystallization time and a large amount of surfactant (SiO_2/N^+ = 3.33 in the synthesis gel). A significantly large portion of surfactant could be wasted without participation as SDA under this condition, as reported by Choi et al.[22] The remainder of the surfactant can be used as a layer to stabilize the hydrophobic surfactant tails participating in the formation of nanosheets, facing tail-to-tail as in the surfactant bilayer.

Synthesis of Unilamellar MFI under a Na^+-Rich Condition. Entry 3 in Table 1 is a synthesis condition that was used for the generation of multilamellar MFI nanosheets in previous works.[22,23] The gel composition was 100 SiO_2:10 $C_{22-6-6}Br_2$:1 Al_2O_3:30 Na_2O:18 H_2SO_4:4000 H_2O. Water glass was used as a silica source. Sodium aluminate was the alumina source. The C_{22-6-6} surfactant used was in the bromide form. Under this Na^+-rich synthesis condition, the multilamellar MFI zeolite

phase was generated by way of three consecutive mesophases:[23] a MCM-41-like hexagonal H_1 phase,[27] KIT-1-like disordered phase,[28] and MCM-50-like lamellar L_α phase.[29] All of these intermediate mesophases exhibited no atomic order in their aluminosilicate frameworks. The multilamellar zeolite product began to form after approximately 3 d under the present synthesis condition at 150 °C. The product reached full crystallinity at 5 d. This product remained without further transformation up to 10 d. No product analysis was performed by XRD beyond 10 d, as the surfactant decomposition was in a basic condition. The pH of this synthesis mixture (gel) was initially 12.

When the pH of the synthesis gel was lowered to 11.4 by changing 18 H_2SO_4 to 24 H_2SO_4 in the gel composition (entry 4 in Table 1), a unilamellar MFI zeolite was obtained in 3 d. This product was maintained without transformation to the multilamellar phase up to 10 d at 150 °C. As shown in the electron micrographs in Figure 4, the zeolite product was obtained as a disordered assembly of 2.0 nm thick nanosheets with narrow $a-c$ planes. The BET surface area was 660 $m^2\ g^{-1}$, and the total pore volume was 1.0 $cm^3\ g^{-1}$. As this result shows, unilamellar MFI nanosheets could be obtained when the pH was lower, even under high Na^+ concentrations. That is, the unilamellar−multilamellar transformation could be suppressed under these low pH conditions. Hence, the generation of multilamellar MFI products reported by Choi et al.[22] may not have been due to a thermodynamic effect of Na^+ ions favoring the formation of the multilamellar mesophase.

The effect of changing the surfactant amount in the synthesis composition was verified in the range of 5−15 $C_{22-6-6}Br_2$ after changing the amount of sulfuric acid to 24 H_2SO_4. The resultant products showed a maximum BET surface area (630−660 $m^2\ g^{-1}$) around 7.5−10 $C_{22-6-6}Br_2$. The total pore volume also reached a maximum (1.0−1.1 $cm^3\ g^{-1}$) in this range. The zeolite yield based on silica recovery was approximately 93%. On the basis of this result and considering the cost efficiency, 7.5 $C_{22-6-6}Br_2$ was the optimum amount of surfactant. The same mole ratios were tested with shorter alkyl surfactants of $C_{12-6-6}Br_2$ and $C_{16-6-6}Br_2$ (entries 5, 6 in Table 1). This also resulted in high-quality unilamellar MFI products. The overall morphologies of the products were nearly identical to those for the unilamellar zeolite obtained from $C_{22-6-6}Br_2$. Figure 5 shows N_2 adsorption isotherms and corresponding pore size distributions of the three unilamellar zeolite products shown in entries 4, 5, and 6 in Table 1. All the zeolites exhibited type-IV N_2 adsorption isotherms, showing a capillary condensation around the relative pressure range between 0.5 and 0.7. This is a typical

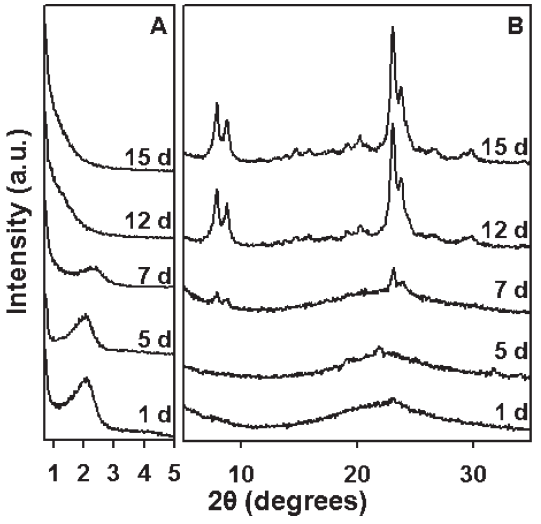

Figure 3. Small-angle (A) and wide-angle (B) powder XRD patterns of MFI zeolite nanosheets in the as-synthesized form periodically taken from the synthesis gel composition of 15 $C_{16-6-6}(OH)_2$:100 SiO_2:1 Al_2O_3:3 H_2SO_4:6000 H_2O after various hydrothermal reaction times.

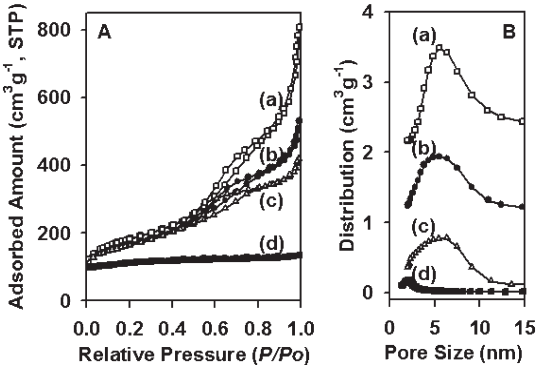

Figure 5. N_2 adsorption isotherms and corresponding pore size distributions for MFI zeolite nanosheets synthesized from the gel composition of 7.5 $C_{n-6-6}(Br^-)_2$:100 SiO_2:1 Al_2O_3:30 Na_2O:24 H_2SO_4:4000 H_2O in Table 1, where n is varied with 22 (a), 16 (b), and 12 (c), respectively. For comparison, the N_2 adsorption data (d) of conventional MFI zeolite are provided. The pore size distributions for (a) and (b) are vertically offset by 2 and 1 $cm^3\ g^{-1}$, respectively.

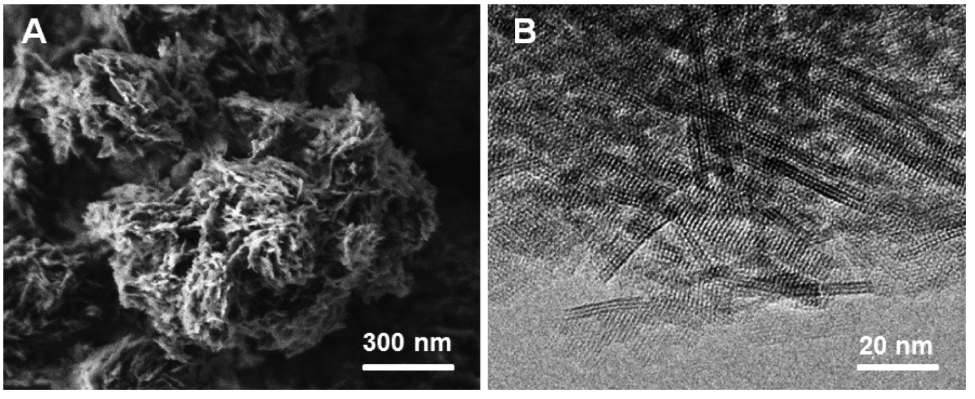

Figure 4. SEM (A) and TEM (B) images of MFI zeolite nanosheets after calcination synthesized from the gel composition of 7.5 $C_{22-6-6}Br_2$:100 SiO_2:1 Al_2O_3:30 Na_2O:24 H_2SO_4:4000 H_2O in Table 1.

dx.doi.org/10.1021/cm103245m |Chem. Mater. 2011, 23, 1273–1279

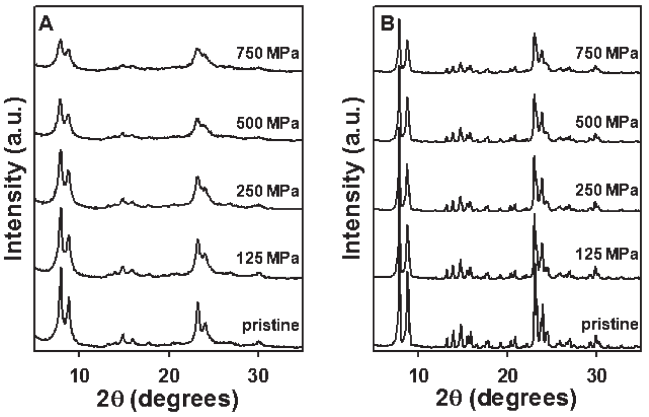

Figure 6. Powder XRD patterns of MFI zeolite nanosheets (A) and bulk MFI zeolite (B) analyzed after different external pressures ranging from 0 to 750 MPa.

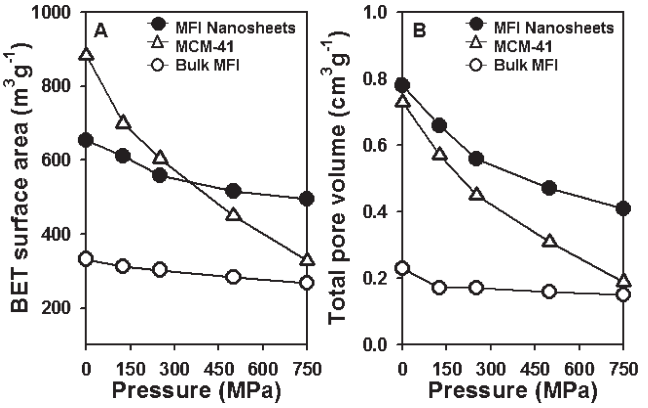

Figure 7. Mechanical stability test on MFI zeolite nanosheets, MCM-41, and bulk MFI zeolite showing the decreasing tendencies of the BET surface area (A) and the total pore volume (B), according to different external pressures ranging from 0 to 750 MPa.

characteristic of disordered mesoporous structure. The broad distribution of mesopore diameters indicates that the MFI zeolite nanosheets were assembled in a fully disordered manner. The BET surface areas and total pore volumes decreased somewhat as the surfactant tail lengths decreased, as shown in Table 1. Nevertheless, the quantities were still much more than those of the bulk MFI zeolite (400 $m^2\ g^{-1}$, 0.23 $cm^3\ g^{-1}$). When Al was incorporated into the gel composition when the Si/Al ratio exceeded 50, the unilamellar zeolite was obtained in 2 d at 150 °C. Longer reaction times were required as the Si/Al ratio decreased further with sodium aluminate. However, the reaction time for unilamellar zeolite decreased to 10 d when $Al_2(SO_4)_3 \cdot 18\ H_2O$ was used instead of sodium aluminate with TEOS used as the silica source (entry 8 in Table 1). The product synthesized with high Al content (entry 8) exhibited a high BET surface area (578 $m^2\ g^{-1}$) but relatively a small pore volume (0.50 $cm^3 g^{-1}$) as compared to high-silica unilamellar zeolite products. This can be explained with decreasing nanosheet sizes as the Al content increases, which was confirmed by TEM (not shown). The nanosheet thickness did not change, and hence, the BET surface area did not decrease. The total pore volume was believed to decrease due to a decrease of void space when the nanosheets were assembled in a fully disordered manner.

Mechanical Stability of Unilamellar MFI Zeolite. A pure silica unilamellar zeolite sample was synthesized, as shown in entry 4 in Table 1, excluding the alumina source. This sample was calcined at 550 °C for 3 h and pressed for 10 min in a stainless steel die, as described in Experimental Section. The mechanical stability of the zeolite framework was judged from the loss of the wide-angle XRD peak intensities that occurred due to the compression. In addition, the mechanical stability of the inter-sheet mesopores was judged from the losses in the BET surface area and pore volume, as analyzed from the N_2 adsorption. These data were compared to data obtained from MCM-41 and bulk MFI zeolite samples with the same mechanical compression. The XRD patterns are displayed as a function of the mechanical pressure in Figure 6. The BET area and pore volume are displayed in Figure 7. These results indicate that the zeolite framework and the pores were progressively damaged as the mechanical pressure increased to 750 MPa. Nevertheless, the zeolite nanosheets were much more stable than the mesoporous system in MCM-41. MCM-41 lost its mesopore volume almost completely at 750 MPa, as indicated in Figure 6. On the other hand, no more than 50% of the pore volume of the nanosheet sample was lost. The low stability of MCM-41 is likely due to the noncrystalline nature of the mesopore walls. The unilamellar zeolite exhibited somewhat low mechanical stability compared to the bulk zeolite. Nevertheless, the stability can be considered to be very high considering its extremely thin framework. It is noteworthy that the unilamellar MFI zeolite exhibited twice the BET surface area and a larger total pore volume compared to the bulk MFI after these samples were compressed at 750 MPa.

■ CONCLUSION

It was possible to synthesize MFI zeolite nanosheets with a thickness of 2 nm as a fully disordered assembly possessing a large mesopore volume between neighboring nanosheets using the $C_{22}H_{45}-N^+(CH_3)_2-C_6H_{12}-N^+(CH_3)_2-C_6H_{13}$-type surfactant as the zeolite structure-directing agent. The disordered assembly was obtained even under synthesis conditions using the bromide form of the surfactant and a sodium-containing silica source such as water glass. The disordered assembly of MFI zeolite nanosheets could be generated in 3 d at 150 °C from a gel composition of 100 SiO_2:7.5 $C_{22-6-6}Br_2$:1 Al_2O_3:30 Na_2O:24 H_2SO_4:4000 H_2O. The zeolite had very a high BET surface area (up to 660 $m^2\ g^{-1}$), a large total pore volume (up to 1.1 $cm^3\ g^{-1}$), and high mechanical stability. Similar results were obtained with variations of the $C_{22}H_{45}$ alkyl chain ranging from $C_{12}H_{25}$ to $C_{16}H_{33}$. This type of zeolitic material is now readily available as a catalytic material, an adsorbent, and a host for nanoparticles, using the synthesis information provided in this work. Furthermore, the present information pertaining to the crystal ripening process would be useful for further studies of the mechanism of ultrathin zeolite generation with structure-directing surfactants. The synthesis of zeolite using a structure-directing surfactant remains limited to MFI nanosheets, but synthesis of MFI or other zeolite frameworks in various nanomorphologies should be possible in principle.

■ AUTHOR INFORMATION

Corresponding Author

*E-mail: rryoo@kaist.ac.kr.

■ ACKNOWLEDGMENT

This work was supported by the National Honor Scientist Program (20100029665) and World Class University Program (R31-2010-000-10071-0) of the Ministry of Education, Science and Technology in Korea.

■ REFERENCES

(1) Cundy, C. S.; Cox, P. A. *Chem. Rev.* **2003**, *103*, 663.
(2) International Zeolite Association Home Page. http://www.iza-online.org/.
(3) Corma, A. *Chem. Rev.* **1997**, *97*, 2373.
(4) Corma, A. *J. Catal.* **2003**, *216*, 298.
(5) Egeblad, K.; Christensen, C. H.; Kustova., M.; Christensen, C. H. *Chem. Mater.* **2008**, *20*, 946.
(6) Tosheva, L.; Valtchev, V. P. *Chem. Mater.* **2005**, *17*, 2494.
(7) Müller, M.; Harvey, G.; Prins, R. *Microporous Mesoporous Mater.* **2000**, *34*, 135.
(8) Ogura, M.; Shinomiya, S.-Y.; Tateno, J.; Nara, Y.; Kikuchi, E.; Matsukata, M. *Chem. Lett.* **2000**, *29*, 882.
(9) Groen, J. C.; Bach, T.; Ziese, U.; Donk, A. M. P.; de Jong, K. P.; Moulijn, J. A.; Pérez-Ramírez, J. *J. Am. Chem. Soc.* **2005**, *127*, 10792.
(10) Groen, J. C.; Moulijn, J. A.; Pérez-Ramírez, J. *J. Mater. Chem.* **2006**, *16*, 2121.
(11) Jacobsen, C. J. H.; Madsen, C.; Houzvicka, J.; Schmidt, I.; Carlsson, A. *J. Am. Chem. Soc.* **2000**, *122*, 7116.
(12) Yang, Z.; Xia, Y.; Mokaya, R. *Adv. Mater.* **2004**, *16*, 727.
(13) Tao, Y.; Kanoh, H.; Kaneko, K. *J. Am. Chem. Soc.* **2003**, *125*, 6044.
(14) Tao, Y.; Kanoh, H.; Abrams, L.; Kaneko, K. *Chem. Rev.* **2006**, *106*, 896.
(15) Holland, B. T.; Abrams, L.; Stein, A. *J. Am. Chem. Soc.* **1999**, *121*, 4308.
(16) Wang, H.; Pinnavaia, T. J. *Angew. Chem., Int. Ed.* **2006**, *45*, 7603.
(17) Choi, M.; Cho, H. S.; Srivastava, R.; Venkatesan, C.; Choi, D. -H.; Ryoo, R. *Nat. Mater.* **2006**, *5*, 718.
(18) Srivastava, R.; Choi, M.; Ryoo, R. *Chem. Commun.* **2006**, 4489.
(19) Cho, K.; Cho, H. S.; de Ménorval, L.-C.; Ryoo, R. *Chem. Mater.* **2009**, *21*, 5664.
(20) Kim, J.; Choi, M.; Ryoo, R. *J. Catal.* **2010**, *269*, 219.
(21) Shetti, V. N.; Kim, J.; Srivastava, R.; Choi, M.; Ryoo, R. *J. Catal.* **2008**, *254*, 296.
(22) Choi, M.; Na, K.; Kim, J.; Sakamoto, Y.; Terasaki, O.; Ryoo, R. *Nature* **2009**, *461*, 246.
(23) Na, K.; Choi, M.; Park, W.; Sakamoto, Y.; Terasaki, O.; Ryoo, R. *J. Am. Chem. Soc.* **2010**, *132*, 4169.
(24) Ryoo, R.; Kim, J. M. *J. Chem. Soc. Chem. Commun.* **1995**, 711.
(25) Heitmann, G. P.; Dahlhoff, G.; Hölderich, W. F. *J. Catal.* **1999**, *186*, 12.
(26) Springuel-Huet, M.-A.; Bonardet, J. -L.; Gédéon, A.; Yue, Y.; Romannikov, V. N.; Fraissard, J. *Microporous Mesoporous Mater.* **2001**, *44*−*45*, 775.
(27) Kresge, C. T.; Leonowicz, M. E.; Roth, W. J.; Vartuli, J. C.; Beck, J. S. *Nature* **1992**, *359*, 710.
(28) Ryoo, R.; Kim, J. M.; Ko, C. H.; Shin, C. H. *J. Phys. Chem.* **1996**, *100*, 17718.
(29) Beck, J. S.; Vartuli, J. C.; Roth, W. J.; Leonowicz, M. E.; Kresge, C. T.; Schmitt, K. D.; Chu, C. T.-W.; Olson, D. H.; Sheppard, E. W.; McCullen, S. B.; Higgins, J. B.; Schlenker, J. L. *J. Am. Chem. Soc.* **1992**, *114*, 10834.